J|A|C|S ARTICLES

Published on Web 08/03/2009

Characteristic Spin−Orbit Induced $^1H(CH_2)$ Chemical Shifts upon Deprotonation of Group 9 Polyamine Aqua and Alcohol Complexes

Marja Hyvärinen,[†] Juha Vaara,[†,‡] Anna Goldammer,[§] Barbara Kutzky,[§] Kaspar Hegetschweiler,*[,§] Martin Kaupp,*[,∥] and Michal Straka*[,⊥]

Laboratory of Physical Chemistry, P.O. Box 55 (A.I. Virtasen aukio 1), University of Helsinki, FIN-00014, Helsinki, Finland, NMR Research Group, Department of Physical Sciences, P.O. Box 3000, FIN-90014, University of Oulu, Finland, Universität des Saarlandes, Anorganische Chemie, Postfach 15 11 50, D-66041 Saarbrücken, Germany, Universität Würzburg, Am Hubland, D-97074 Würzburg, Germany, and Institute of Organic Chemistry and Biochemistry, Academy of Sciences of the Czech Republic, Flemingovo n. 2., CZE-16610, Praha 6, Czech Republic

Received May 12, 2009; E-mail: hegetschweiler@mx.uni-saarland.de; kaupp@mail.uni-wuerzburg.de; straka@uochb.cas.cz

Abstract: The recently observed nonintuitive pH dependence of methylene ^1H chemical shifts in cobalt(III) polyamine complexes upon deprotonation of coordinated aqua or (poly)alcohol coligands (*J. Am. Chem. Soc.* **2004**, *126*, 6728) was attributed to differential spin−orbit effects on the ^1H shifts transmitted over three bonds from the cobalt low-spin d^6 center. These remarkably large spin−orbit effects due to the comparably light Co center have now been examined closely by comparative computations for homologous Rh and Ir complexes, as well as by NMR titrations for a Rh complex. While larger spin−orbit effects (proportional to Z^2) would have been expected for the heavier metal centers, the characteristic ^1H deshieldings upon deprotonation of $[Rh(tren)(OH_2)_2]^{3+}$ [tren = tris(2-aminoethyl)-amine] turn out to be *smaller* than for the Co homologous Co complex. Systematic computational studies ranging from smaller models to the full complexes confirm these results and extend them to the Ir homologues. Closer analysis indicates that the spin−orbit shift contributions do not follow the expected Z^2 behavior but are modulated dramatically by increasing energy denominators in the perturbation expressions. This is related to the increasing ligand-field splitting from 3d to 4d to 5d system, leading to almost identical differential spin−orbit shifts for the Co and Rh complexes and to only moderately larger effects for the Ir complex (by a factor of about two). Moreover, the differential nonspin−orbit deprotonation shifts cancel the spin−orbit induced contributions largely in the Rh complex, leading to the experimentally observed inverted behavior. The full multidentate polyamine complexes studied experimentally exhibit different three- and four-bond Fermi-contact pathways for transmission of the spin−orbit ^1H shifts. The novel four-bond pathways have different conformational dependencies than the Karplus-like three-bond pathways established previously. Both types of contributions are of similar magnitude. The ^1H NMR deprotonation shift patterns of $[Ir(tren)(OH_2)_2]^{3+}$ have been predicted computationally.

1. Introduction

In detailed ^1H NMR titrations of cobalt polyamine complexes, we have recently observed an unexpected, characteristic *deshielding* of some of the $^1H(CH_2)$ chemical shifts upon deprotonation of a coordinated aqua or (poly)alcohol coligand.[1] These nonintuitive deprotonation shifts were only observed for CH_2 groups bonded to the amine nitrogen in *trans* position to the deprotonated coligand, and only for an essentially antiperiplanar arrangement of the Co−N−C−H bond pathway involved (see, e.g., the positive slopes for the shifts of H_A, H_B, and H_C of $[Co(tren)(OH_2)_2]^{3+}$ in Figure 1 (bottom). All other proton shifts *decreased* upon deprotonation, as one would expect from the improved donor ability of deprotonated hydroxo or alcoholato coligand, see H_E and H_F in Figure 1 (bottom). The unprecedented deprotonation shift patterns bear substantial potential for stereochemical analysis and thus have been analyzed by quantum-chemical calculations using density functional theory (DFT) with explicit third-order perturbation theory corrections for spin−orbit contributions.[1] It turned out that nonrelativistic calculations gave more shielding upon deprotonation for all $^1H(CH_2)$ positions and, thus, could not explain the nonintuitive deshielding for some of the protons. Only after inclusion of spin−orbit (SO) corrections, the differential SO shifts reverted the trend for the indicated protons in the *trans* CH_2 groups in antiperiplanar position. Closer analysis revealed that the SO effects arise from

[†] University of Helsinki.
[‡] University of Oulu.
[§] Universität des Saarlandes.
[∥] Universität Würzburg.
[⊥] Academy of Sciences of the Czech Republic.

(1) Hegetschweiler, K.; Kuppert, D.; Huppert, J.; Straka, M.; Kaupp, M. *J. Am. Chem. Soc.* **2004**, *126*, 6728.

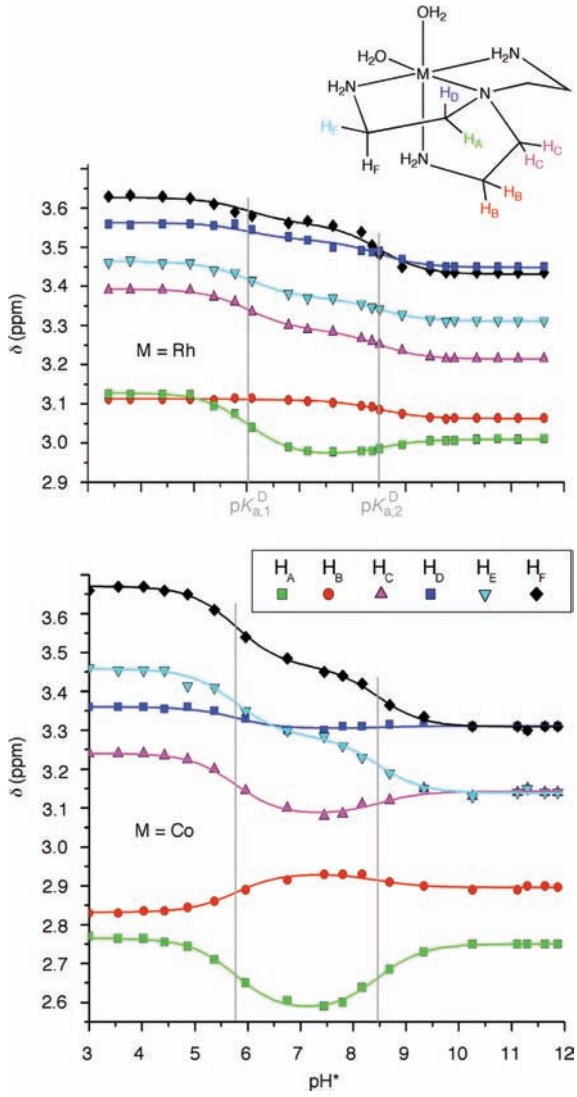

Figure 1. pH* dependence[9] of the ^{1}H NMR resonances of [Rh(tren)$(H_2O)_2]^{3+}$ **1[Rh$(H_2O)_2]^{3+}$** (top) and [Co(tren)$(H_2O)_2]^{3+}$ **1[Co$(H_2O)_2]^{3+}$** (bottom), together with a representation of the molecular structure and the labeling scheme. The points correspond to the experimental values, lines are fitted (minimization of $\Sigma[\delta_{obs} - \delta_{calc}]^2$), assuming a rapid equilibrium between the variably protonated species.

the central Co atom and demonstrated a Karplus-type conformational dependence of the three-bond SO contributions, thus explaining the large SO effects for antiperiplanar positions. Moreover, the notable *differential* SO effects on the deprotonation shifts in *trans* position were found to be caused by appreciably reduced SO shifts in the deprotonated complex due to an interruption of the transfer pathway for the SO-induced spin density (a result of a weakened *trans* Co−N bond).[1] Detailed understanding of these ^{1}H deprotonation shifts and their stereoelectronic background opens possibilities of using these effects in NMR-based structure determination of polyalcohols, for example, for carbohydrates. Improved understanding may even aid the assignment of signals to specific proton positions without 2D experiments.

While much larger SO effects on NMR shifts are known,[2−6] the differential pH-dependent SO shifts in these cobalt polyamine complexes remain peculiar for several reasons. Apart from the above-mentioned pronounced and potentially useful stereochemical dependence, the appreciable magnitude of a three-bond SO effect on a proton shift (up to almost one ppm[1]) is striking, considering that it arises solely due to SO splitting of the comparably light Co center ($Z = 27$). In fact, the effect is significantly larger than the three-bond SO effects (ca. 0.3 ppm) computed for β-^{1}H shifts in iodoethane, caused by the much heavier iodine substituent ($Z = 53$).[6] This contradicts the usual expectation of a general Z^2 dependence of SO effects.

We rationalized this by rather small, squared energy denominators in the third-order perturbation expressions for the SO chemical shifts[1] (see below). Hence, the question arises, what may be expected when replacing cobalt by its heavier homologues Rh and Ir. Will a Z^2 dependence of SO chemical shifts prevail, or will changes in the energy denominators play an important role? If characteristic stereochemical dependencies also pertain to complexes of the heavier metal centers, these might be useful in their own right. We have therefore extended the experimental and quantum-chemical investigations to Rh and Ir complexes. That is, we provide detailed ^{1}H NMR titration experiments for $[Rh^{III}(tren)(OH_2)_2]^{3+}$ (**1[Rh$(H_2O)_2]^{3+}$**, tren = tris(2-aminoethyl)-amine) in comparison with its Co analogue $[Co(tren)(OH_2)_2]^{3+}$ (**1[Co$(H_2O)_2]^{3+}$**).[1] **1[Rh$(H_2O)_2]^{3+}$** is a known complex,[7,8] which forms one single stereoisomer with a rather rigid structure, making it suitable for our purposes. Surprisingly enough, we find the nonintuitive deshielding deprotonation shifts of **1[Rh$(H_2O)_2]^{3+}$** to be substantially smaller than those for **1[Co$(H_2O)_2]^{3+}$** or even absent. Therefore, a detailed computational study of homologous series of Co, Rh, and Ir complexes has been carried out, ranging from small models, intended to isolate particular stereoelectronic contributions to the observed shift trends in the NMR titrations, to the full target tren complexes. Not only do we find the dependence of the SO effects on atomic number to differ dramatically from the usual Z^2 dependence, but the computations also uncover a new four-bond pathway that contributes to the unusual SO chemical shift effects in these chelate complexes.

2. Experimental and Computational Methods and Materials

a. Experimental Methods. Materials. $RhCl_3 \cdot 3H_2O$ (Merck), LiOH (Fluka), tris(2-aminoethyl)-amine (Fluka), and $AgCF_3SO_3$ (Acros Organics) were commercially available and used as obtained. Dowex 50 W-X2 cation-exchange resin (100−200 mesh, H^+ form) was purchased from Fluka and conditioned by excessive rinsing with 6 M HCl and H_2O prior to use. SP-Sephadex C-25 cation exchange resin (200 mesh, from Pharmacia Biotech) was converted into the Na^+-form by elution with a 2 M NaCl solution prior to

(2) Relativistic Effects on NMR Chemical Shifts. Kaupp, M. In *Relativistic Electronic Structure Theory II: Applications*; Schwerdtfeger, P., Ed.; Theoretical and Computational Chemistry; Elsevier: Amsterdam, 2004.
(3) *Calculation of NMR and EPR Parameters. Theory and Applications*; Kaupp, M., Bühl, M., Malkin, V. G., Eds.; Wiley-VCH: Weinheim, 2004.
(4) Kaupp, M. Interpretation of NMR Chemical Shifts. In *Calculation of NMR and EPR Parameters. Theory and Applications*; Kaupp, M., Bühl, M., Malkin, V. G., Eds.; Wiley-VCH: Weinheim, 2004; Ch. 18, p 293.
(5) Vaara, J.; Manninen, P.; Lantto, P. Perturbational and ECP Calculation of Relativistic Effects in NMR Shielding and Spin-Spin-Coupling. In *Calculation of NMR and EPR Parameters. Theory and Applications*; Kaupp, M., Bühl, M., Malkin, V. G., Eds.; Wiley-VCH: Weinheim, 2004; Ch. 13, p 209.
(6) Kaupp, M.; Malkina, O. L.; Malkin, V. G.; Pyykkö, P. *Chem.—Eur. J.* **1998**, *4*, 118.
(7) Martins, E.; Sheridan, P. S. *Inorg. Chem.* **1978**, *17*, 2822.
(8) Saliby, M. J.; Kaplan, E. B.; Sheridan, P. S.; Madan, S. K. *Inorg. Chem.* **1981**, *20*, 728.

use and sufficient rinsing with H_2O until the eluent was free of chloride (checked with $AgNO_3$). Tris(2-aminoethyl)-amine-trihydrochloride (tren·3HCl) was prepared from tren (17.34 g, 119 mmol) and concentrated hydrochloric acid (30 mL) in EtOH (60 mL) at 0 °C. The white solid (93%) was recrystallized from EtOH/H_2O (1:1) and dried in vacuo. C,H,N-analysis of this product was in agreement with the composition of $C_6H_{21}N_4Cl_3$.

Instrumentation. ^1H and $^{13}C\{^1H\}$ NMR spectra were measured in D_2O (21 °C) using a Bruker Avance Ultrashield 400 spectrometer (resonance frequencies: 400.13 MHz for ^1H and 100.6 MHz for ^{13}C). Chemical shifts (in ppm) are given relative to sodium (trimethylsilyl)propionate-d^4 as an internal standard (= 0 ppm). A Hamilton SPINTRODE glass electrode, fitted with an internal Ag/AgCl reference (H_2O), which was calibrated with aqueous (H_2O) buffer solutions, was used to measure the pH* value[9] directly within the NMR tube. The pH* was adjusted by adding appropriate amounts of $DClO_4$ or NaOD dissolved in D_2O and was checked prior to and after each measurement. The buffering capacity of the Rh complex proved to be sufficient to guarantee a suitable pH*. The use of an additional buffer was therefore not necessary. Two-dimensional NMR experiments were performed according to the literature.[10] The ^1H NMR chemical shifts of the individual resonances were resolved by modeling the entire spin system using the computer program *WIN-DAISY*.[11] An example for pH* 3.4 and pH* 12.1 is shown in Supporting Information (Figure S1). The titration curves δ versus pH* were fitted by least-squares calculations ($\Sigma[\delta_{obs} - \delta_{calc}]^2 = \min$) using the computer program *NMR-Tit*.[12] The resulting parameters[13] (pK_a and δ_{calc}) of the macro species[13] are collected in Table S1 (Supporting Information).

Ag^+ monitoring in the reaction mixture was performed using a Ag electrode with an incorporated Ag/AgCl reference (Metrohm). UV/vis spectra were measured at ambient temperature using an immersion probe (HELLMA), which was connected to a diode array spectrophotometer (J&M, TIDAS-UV/NIR/100−1). Mass spectra (ESI+) were recorded on a ZQ 4000 (Waters) device. C,H,N analysis was performed by Anton Zaschka, (Saarland University) on a vario EL analyzer (Elementare Analysesysteme GmbH, Hanau).

***cis*-Dichloro-(β,β',β''-triaminoethylamine)-rhodium(III).** The chloride salt of this complex, *cis*-$[Rh(tren)Cl_2]Cl$, was prepared according to a previously published protocol[14] which was applied with some minor modifications: $RhCl_3 \cdot 3H_2O$ (2.00 g, 7.6 mmol), tren·3HCl (1.95 g, 7.5 mmol) and $LiOH \cdot H_2O$ (0.3 g, 7.1 mmol) were dissolved in 100 mL of H_2O and refluxed until a clear solution was obtained. Over a period of 1 h a solution of LiOH (0.65 g, 15 mmol in 100 mL of H_2O) was added dropwise to the refluxing reaction mixture until a pH of about 7 was reached (checked with indicator paper). During this procedure, a yellow byproduct of unknown composition precipitated which was removed by filtration and discarded. The clear filtrate was concentrated up to a total volume of 20 mL, and acidified with aqueous HCl to a pH of about 2. The solution was sorbed on Dowex 50, and the remaining tren·3HCl together with LiCl was removed with 0.5 M HCl. The Rh complex was then eluted with 1 M HCl. The complex-containing fraction was evaporated to dryness, dissolved in H_2O, sorbed on Sephadex C-25, and eluted with 0.04 M Na_2SO_4. Two yellow bands emerged. The first band, containing the desired $[Rh(tren)Cl_2]^+$, was collected and desalted on Dowex 50. The second band, containing a species with a partially coordinating tren ligand, was discarded. Yield 0.72 g (27%) of a bright-yellow solid. Elemental analysis (%) calcd for $C_6H_{18}N_4Cl_3Rh$: C 20.27; H 5.10; N 15.76, found: C 19.82; H 5.23; N 15.21. UV/vis: λ_{max} [nm] 297, 362. MS (ESI+): m/z = 319 (100%), 321 (65%), 323 (11%). This intensity distribution is in agreement with the calculated isotope pattern of $C_6H_{18}N_4Cl_2Rh^+$. ^1H NMR: δ = 3.00, 3.17, 3.37, 3.45, 3.91 (ddd, 10H) 3.59 (m, 2H) 5.12, 5.27, 5.69 (NH_2, 6H). ^{13}C NMR: δ = 49.8, 50.2, 63.2, 66.2. A part of this sample was converted into the tetrachlorozincate salt by dissolving it in a minimal amount of 3 M aquous HCl and adding an excess of $ZnCl_2$ (dissolved in 6 M aqueous HCl). The mixture was kept for two days at 4 °C and the resulting solid was filtered. Single crystals of composition $[Rh(tren)Cl_2]_2[ZnCl_4] \cdot 2H_2O$ suitable for an X-ray structure analysis were grown by recrystallization from H_2O.

***cis*-Diaqua-(β,β',β''-triaminoethylamine)-rhodium(III).** To a solution of $[Rh(tren)Cl_2]Cl$ (0.5 g, 1.4 mmol, dissolved in 30 mL of H_2O), $AgCF_3SO_3$ was added (1.3 g, 5.1 mmol). The resulting suspension was stirred under reflux for 5 h, and solid AgCl was removed by filtration. The remaining Ag^+ was precipitated by controlled addition of 0.1 M HCl, using an Ag electrode for monitoring Ag^+ concentration. The additional solid AgCl was again removed by filtration, and the resulting clear, pale-yellow solution was evaporated to dryness, yielding a bright-yellow, highly hydrophilic solid. UV/vis: λ_{max} [nm] = 277, 323.[15] MS (ESI+): m/z = 433 [17%, $Rh(tren)(OH_2)(OH)(CF_3SO_3)^+$], 415 [24%, $Rh(tren)(OH)(CF_3SO_3)^+$], 397 [22%, $Rh(H_{-1}tren)(CF_3SO_3)^+$]. ^1H NMR: see Figure S1 (Supporting Information). ^{13}C NMR: δ = 48.5, 48.9, 62.1, 64.8, 117.7, 120.9, 124.1, 127.2.

Crystal Structure Analysis. X-ray diffraction data of $[Rh(tren)Cl_2]_2[ZnCl_4] \cdot 2H_2O$ were collected on a Stoe IPDS diffractometer at 200 K, using graphite-monochromated Mo Kα radiation (λ = 0.71073 Å). An empirical absorption correction was applied to the data. The structure was solved using direct methods (SHELXS-97) and refined by full-matrix least-squares calculations on F^2 (SHELXL-97).[16] The hydrogen atomic positions were calculated using a riding model. Crystal data: orthorhombic, space group $P2_12_12_1$, a = 7.1150(10) Å, b = 20.084(4) Å, c = 20.490(4) Å, V = 2928.0(9) Å^3. Z = 4 for $C_{12}H_{40}Cl_8N_8O_2Rh_2Zn$. Of 18402 reflections ($1.99 < \theta < 23.96°$), 4534 were unique ($R_{int}$ = 0.079), and 4280 were observed with $I > 2\sigma(I)$. The refinement of 298 parameters resulted in agreement factors of $R1$ = 0.029 (observed data) and w$R2$ = 0.070 (all data). In Supporting Information, Table S2 gives additional crystallographic information, and Figure S2 provides a display of the molecular structure and a list of selected bond lengths and angles.

b. Computational Methods. Structure Optimizations. Structures were optimized with the Turbomole 5.9.1 program[17] at the density functional theory (DFT) level using the BP86 functional[18,19] and def2-TZVPP basis sets.[20] For cobalt and the ligand atoms (C, N, O, H), def2-TZVPP provides all-electron basis sets, while for

(9) pH* refers to the direct pH-meter reading for a pH electrode which has been calibrated in aqueous (H_2O) media. For the transformation of pH* into pD see: (a) Delgado, R.; Frausto Da Silva, J. J. R.; Amorim, M. T. S.; Cabral, M. F.; Chaves, S.; Costa, J. *Anal. Chim. Acta* **1991**, *245*, 271. (b) Lumry, R.; Smith, E. L.; Glantz, R. R. *J. Am. Chem. Soc.* **1951**, *73*, 4330.

(10) (a) Hurd, R. E. *J. Magn. Reson.* **1990**, *87*, 422. (b) von Kienlin, M.; Moonen, C. T. W.; van der Toorn, A.; van Zijl, P. C. M. *J. Magn. Reson.* **1991**, *93*, 423. (c) Hurd, R. E.; John, B. K. *J. Magn. Reson.* **1991**, *91*, 648. (d) Ruiz-Cabello, J.; Vuister, G. W.; Moonen, C. T. W.; van Gelderen, P.; Cohen, J. S.; van Zijl, P. C. M. *J. Magn. Reson.* **1992**, *100*, 282. (e) Willker, W.; Leibfritz, D.; Kerssebaum, R.; Bermel, W. *Magn. Reson. Chem.* **1993**, *31*, 287.

(11) Weber, U.; Spiske, R.; Höffken, H. W.; Hägele, G.; Thiele, H. *WIN-DAISY, Program for Simulation and Iteration of High Resolution NMR Spectra*; University of Düsseldorf: Düsseldorf, 1993.

(12) Ries, A.; Hegetschweiler, K. NMR-Tit, *Program for the Simulation of pH Dependent Shifts in NMR Spectra*, Version 2.0, Saarbrücken: 1999.

(13) Martell, A. E.; Motekaitis, R. J. *Determination and Use of Stability Constants*, 2nd ed.; VCH: New York, 1992.

(14) Johnson, S. A.; Basolo, F. *Inorg. Chem.* **1962**, *1*, 925.

(15) Martins, E.; Sheridan, P. S. *Inorg. Chem.* **1978**, *17*, 2822.

(16) Sheldrick, G. M. *Acta Crystallogr., Sect. A* **2008**, *64*, 112.

(17) Ahlrichs, R.; Bär, M.; Häser, M.; Horn, H.; Kölmel, C. *Chem. Phys. Lett.* **1989**, *162*, 165.

(18) Becke, A. D. *Phys. Rev. A* **1988**, *38*, 3098.

(19) Perdew, J. P. *Phys. Rev. B* **1986**, *33*, 8822.

(20) Weigend, F.; Ahlrichs, R. *Phys. Chem. Chem. Phys.* **2005**, *7*, 3297.

rhodium and iridium, energy-adjusted quasirelativistic small-core effective-core potentials (ECP) with appropriate valence basis sets are used.[21]

Calculation of Chemical Shifts. Nonrelativistic (NR) and scalar relativistic (SR) nuclear magnetic shielding tensors were calculated with the Gaussian 03 program[22] using gauge-including atomic orbitals (GIAO) to deal with the gauge invariance problem. Inclusion of SR effects was limited to the use of quasirelativistic ECPs, that is, passive relativistic corrections of the wave function. Calculations of SO corrections to the nuclear shielding tensors used a combined finite-perturbation/sum-over-states density-functional perturbation theory (SOS-DFPT) triple perturbation approach[23,24] with a finite Fermi contact perturbation equal to $\lambda = 0.0005$ at the hydrogen atom under study. A common gauge origin placed at the metal center was employed. The size of perturbation λ in the triple perturbation approach was carefully checked. Values between 10^{-3} and 10^{-5} a.u. provided a plateau with shift variations within 0.01 ppm. The one- and two-electron SO contributions were treated simultaneously by the effective one-electron, one-center mean-field approximation[25] as implemented in the AMFI program.[26] The Fermi contact-perturbed orbitals were calculated in the Gaussian 03 code and transferred to the in-house developed MASTER code[23,24,27] using the Gaussian-to-MASTER interface.[28] The MASTER code is limited to use of s, p, and d functions. Hence, f and g functions (where present) were removed from the original basis sets in the SO shielding calculations. For details on the basis sets, see Supporting Information, Table S3. The GGA (general-gradient approximation) density functionals PBE,[29] BP86,[18,19] PW91,[30] and BLYP, accessible in MASTER, provide all very similar results for the NR and SR shifts (pseudopotentials with averaged spin−orbit terms) as well as for the SO contributions (see Table S4 in the Supporting Information).

To evaluate the validity of the approximations made in the MASTER calculations, some additional computations were done with the more recent MAG-ReSpect code.[31] This code allows use of hybrid density functionals, f- and g-type basis functions, and the GIAO approach in the SO-shift computations. Some of the results are detailed in Table S4 in the Supporting Information and may be summarized briefly as follows: (a) the role of the f and g functions was found to be almost negligible for SO shieldings; (b) changing the treatment of the gauge problem from a common gauge origin on the metal center to the more sophisticated GIAO approach provides slightly less negative SO shifts, but the qualitative results and trends remain unchanged; (c) hybrid functionals, too, give numerically different nuclear shieldings but do not alter our qualitative observations for trends in chemical shifts. We neglect the spin-dipolar contribution to the SO shielding constant in calculations. While its contribution is typically much smaller than that of the Fermi contact interaction,[32] and a significant degree of cancellation is expected to occur in the differential shifts, omission of the spin-dipolar contribution may affect the quantitative comparison between the theory and experiment.

Reported results are mainly based on the PBE functional using recently developed multiconfiguration Dirac−Fock (MCDF) ECPs for Co,[33] Rh,[34] and Ir,[34] with the corresponding valence basis sets of VTZPP quality having the (10s9p8d)/[5s5p4d] contraction pattern for Co and Rh,[34] all with f and g functions removed. Corresponding iridium basis sets were not yet available. Hence, we used the decontracted rhodium VTZPP basis set for Ir. For the ligand atoms we used the Huzinaga-III (HIII) basis set[35] with (11s7p2d)/[7s6p2d] and (6s2p)/[4s2p] contractions on O/N/C and H, respectively. Improvement of the basis sets toward VQZPP[34] on the metal and HIV[35] on the ligand atoms did not alter the results significantly (Table S4 in the Supporting Information).

Additional Details. TMS was used as the reference molecule for conversion of the nuclear shielding constants to chemical shifts. A typical value for the ^{1}H shielding constant in TMS is 31.4 ppm (PBE/HIII). The SO effect on ^{1}H in TMS was found below 0.01 ppm and was not considered further. Singlet and triplet excitation energy calculations were carried out using time-dependent density functional theory (TDDFT) with the Gaussian 03 program at the B3LYP hybrid functional level.[36] The same basis sets were used as for the SO shielding calculations.

3. Results and Discussion

a. Experimental ^{1}H NMR Results. The rhodium-tren-diaqua complex **1[Rh(H$_2$O)$_2$]$^{3+}$** was prepared from the corresponding chloro complex [Rh(tren)Cl$_2$]Cl.[7] Since reanation was observed for **1[Rh(H$_2$O)$_2$]$^{3+}$** in chloride containing media,[8] a quantitative removal of Cl^- from the reaction mixture was necessary. The aquation reaction was, therefore, performed at elevated temperature using Ag(CF$_3$SO$_3$) for a quantitative precipitation of chloride and [Rh(tren)(OH$_2$)$_2$]$^{3+}$ (**1[Rh(H$_2$O)$_2$]$^{3+}$**) was then obtained as a very hygroscopic triflate salt. Completeness of the Cl^-/H_2O exchange was checked by UV/vis spectroscopy[7] and by mass spectrometry. In contrast to [Rh(tren)Cl$_2$]$^+$, which exhibited a beautiful, easily assignable ^{1}H NMR spectrum with separated sharp lines for all resonances, the ^{1}H NMR spectrum of the diaqua complex **1[Rh(H$_2$O)$_2$]$^{3+}$** showed relatively broad signals with a significant overlap. Starting assignment of these resonances could be achieved by a series of 2D ^{1}H−^{13}C COSY spectra. For a precise determination of the ^{1}H NMR characteristics, the spin system of this complex was modeled using the computer program *WIN-DAISY*. Individual chemical shifts together with the coupling constants were fitted by a least-squares procedure.[11] A total of 21 spectra were recorded at variable pH* values in the range 3.4−12.6 (Figure 1, top). In analogy to our previous investigation,[1] a rapid equilibrium between the aqua complex **1[Rh(H$_2$O)$_2$]$^{3+}$** and its deprotonation products [Rh(tren)(H$_2$O)(OH)]$^{2+}$ (**1[Rh(OH)(H$_2$O)]$^{2+}$**) and [Rh(tren)(OH)$_2$]$^+$ (**1[Rh(OH)$_2$]$^+$**) was assumed. Consequently,

(21) Andrae, D.; Haeussermann, U.; Dolg, M.; Stoll, H.; Preuss, H. *Theor. Chim. Acta* **1990**, *77*, 123.
(22) Frisch, M. J. et al. *Gaussian 03*, Revision C.02; Gaussian, Inc.: Wallingford, CT, 2004.
(23) Vaara, J.; Malkina, O. L.; Stoll, H.; Malkin, V. G.; Kaupp, M. *J. Chem. Phys.* **2001**, *114*, 61.
(24) Malkina, O. L.; Schimmelpfennig, B.; Kaupp, M.; Hess, B. A.; Chandra, P.; Wahlgren, U.; Malkin, V. G. *Chem. Phys. Lett.* **1998**, *296*, 93. Malkin, V. G.; Malkina, O. L.; Salahub, D. R. *Chem. Phys. Lett.* **1996**, *261*, 335.
(25) Hess, B. A.; Marian, C. M.; Wahlgren, U.; Gropen, O. *Chem. Phys.Lett.* **1996**, *251*, 365.
(26) Schimmelpfennig, B. *Atomic Spin-Orbit Mean-Field Program*; Stockholms Universitet: Sweden, 1996.
(27) MASTER (magnetic property packages for deMon): Malkin, V. G.; Malkina, O. L.; Eriksson, L. A.; Salahub, D. R. In *Modern Density Functional Theory: A Tool for Chemistry*; Theoretical and Computational Chemistry; Seminario, J. M., Politzer, P., Eds.; Elsevier: Amsterdam, 1995; Vol. 2.
(28) Pennanen, T. O.; Vaara, J. *J. Chem. Phys.* **2005**, *123*, 174102.
(29) Perdew, J. P.; Burke, K.; Ernzerhof, M. *Phys. Rev. Lett.* **1996**, *77*, 3865.
(30) Perdew, J. P.; Chevary, J. A.; Vosko, S. H.; Jackson, K. A.; Pederson, M. R.; Singh, D. J.; Fiolhais, C. *Phys. Rev. B* **1992**, *46*, 6671.
(31) Malkin, V. G.; et al. *MAG-ReSpect program*, version 2.1; 2005.
(32) (a) Vaara, J.; Ruud, K.; Vahtras, O.; Ågren, H.; Jokisaari, J. *J. Chem. Phys.* **1998**, *109*, 1212. (b) Straka, M.; Lantto, P.; Räsänen, M.; Vaara, J. *J. Chem. Phys.* **2007**, *127*, 234314.
(33) Dolg, M. *Theor. Chem. Acc.* **2005**, *114*, 297.
(34) Peterson, K. A.; Figgen, D.; Dolg, M.; Stoll, H. *J. Chem. Phys.* **2007**, *126*, 124101.
(35) (a) Huzinaga, S. *Approximate Atomic Functions*; University of Alberta: Edmonton, 1971. (b) Kutzelnigg, W.; Fleischer, U.; Schindler, M. *NMR -Basic Principles and Progress*; Springer: Heidelberg, 1990; Vol. 23, p 165ff.
(36) (a) Becke, A. D. *J. Chem. Phys.* **1993**, *98*, 5648. (b) Lee, C.; Yang, W.; Parr, R. G. *Phys. Rev. B* **1988**, *37*, 785. (c) Miehlich, B.; Savin, A.; Stoll, H.; Preuss, H. *Chem. Phys. Lett.* **1989**, *157*, 200.

Table 1. Comparison of the Differential Chemical Shifts $\Delta\delta$ (in ppm) Induced by the First and the Second Deprotonation of the Two Coordinated Water Molecules of **1[M(H$_2$O)$_2$]$^{3+}$** (M = Co, Rh, Ir)[a]

		1st deprot.	2nd deprot.
H_A	Co	−0.21 (−0.28)	**+0.19** (+0.19)
	Rh	−0.16 (−0.30)	**+0.04** (−0.08)
	Ir	(−0.03)	(+0.08)
H_B	Co	**+0.10** (+0.34)	−0.03 (−0.17)
	Rh	0.00 (−0.16)	−0.05 (−0.17)
	Ir	(0.00)	(−0.05)
H_C	Co	−0.16 (−0.19)	**+0.06** (+0.18)
	Rh	−0.10 (−0.38)	−0.08 (−0.14)
	Ir	(−0.25)	(−0.01)
H_D	Co	−0.06 (−0.25)	**+0.01** (−0.03)
	Rh	−0.04 (−0.03)	−0.07 (−0.42)
	Ir	(+0.04)	(−0.30)
H_E	Co	−0.17 (−0.61)	−0.15 (−0.28)
	Rh	−0.09 (−0.36)	−0.06 (−0.19)
	Ir	(−0.22)	(−0.04)
H_F	Co	−0.20 (−0.56)	−0.16 (−0.12)
	Rh	−0.07 (−0.48)	−0.13 (−0.20)
	Ir	(−0.43)	(−0.03)

[a] Changes with a positive sign are highlighted. Computational gas-phase results (PBE/MDF/VTZPP/HIII level) are given in parentheses. The underlined numbers point to a disagreement in sign between theory and experiment.

the observed chemical shifts were interpreted as weighted averages for the equilibrium composition of **1[Rh(H$_2$O)$_2$]$^{3+}$**, **1[Rh(OH)(H$_2$O)]$^{2+}$**, and **1[Rh(OH)$_2$]$^{+}$**. The lines shown in Figure 1 (top) were calculated accordingly by a least-squares procedure $\Sigma[\delta_{obs} - \delta_{calcd}]^2 = \min$.[12] Similarly to the [Co(tren)(OH$_2$)$_2$]$^{3+}$ complex (**1[Co(H$_2$O)$_2$]$^{3+}$**, Figure 1 (bottom),[1] two distinct buffer regions (5 < pH* < 7 and 7.5 < pH* < 9.5) with pK_a values of 6.03 and 8.50 could be detected in the δ versus pH* curve. Corresponding pK_a values of the Co^{III} complex **1[Co(H$_2$O)$_2$]$^{3+}$** are 5.77 and 8.46. The difference in acidity of these two complexes is only marginal. For the pure aqua ions, however, it is well established that [Co(OH$_2$)$_6$]$^{3+}$ is a considerably stronger acid than [Rh(OH$_2$)$_6$]$^{3+}$.[37]

Interestingly, the ^{1}H resonances of the two complexes **1[M(H$_2$O)$_2$]$^{3+}$**do not exhibit similar δ versus pH* dependence in the two buffer regions. While the hydrogen atoms with a *cis* H−C−N−Rh−O arrangement, such as H_E and H_F get an increasing shielding with increasing deprotonation, the hydrogen atoms having their deprotonated water molecules in a *trans* H−C−N−Rh−O arrangement show a more complex behavior. A comparison of these effects for the two systems clearly shows that the changes of the chemical shifts induced upon deprotonation tend to be larger for the Co complex (Table 1). In particular, the nonmonotonous curves for H_A and H_B are much less bent for the Rh complex, and the curve for H_C has become monotonous, in contrast to **1[Co(H$_2$O)$_2$]$^{3+}$**, where the deprotonation of the aqua ligand leads clearly to a deshielding in *trans* position and to shielding in the *cis* position[1] (the curve for H_D has a clear negative slope everywhere for **1[Rh(H$_2$O)$_2$]$^{3+}$**).

As discussed in ref 1, the SO effects on shielding exhibit strong conformational dependences (cf. below). Unfortunately, a direct comparison of the molecular structure of **1[Rh(H$_2$O)$_2$]$^{3+}$** and **1[Co(H$_2$O)$_2$]$^{3+}$** is not possible. A crystal structure of the triflate salt of **1[Co(H$_2$O)$_2$]$^{3+}$** has been published,[38] but the corresponding structure of **1[Rh(H$_2$O)$_2$]$^{3+}$** is not known. While our efforts to obtain a crystal structure of this complex were not successful, we could grow single crystals of the corresponding chloro complex [Rh(tren)Cl$_2$]$_2$[ZnCl$_4$]. Inspection of the structural features did not reveal significant differences for **1[Co(H$_2$O)$_2$]$^{3+}$** and [Rh(tren)Cl$_2$]$^{+}$.[39] In particular, the relevant configuration of the chelate rings and the corresponding torsional angles of the two complexes are quite similar, although the Rh complex has somewhat longer metal−nitrogen bonds. A superposition of the two structures (best fit of fragments) is shown in Figure S3 in Supporting Information. Therefore, it seems rather unlikely that the different characteristics in the shift patterns upon deprotonation are caused by geometric differences of the two complexes. This is also confirmed by the computational structure optimizations (cf. below), which provide similar structures for Co and Rh complexes with very similar overall shape. Concomitant torsion angles are almost identical in the Co, Rh, and Ir analogues. The M−N and M−O distances are correspondingly larger in the heavier Rh complex (M−N and M−O bonds are in Table 3, typical M−N−C−H torsions can be found in Tables S8−S9 in Supporting Information).

The δ versus pH* curves shown in Figure 1 are indicative for a selective deprotonation scheme for both **1[Co(H$_2$O)$_2$]$^{3+}$** and **1[Rh(H$_2$O)$_2$]$^{3+}$**. Using the SO-induced *trans* effect[1] to locate the deprotonation site (see below), it becomes evident that the H$_2$O molecule *trans* to the primary amino group is more acidic and will be predominantly deprotonated in the first deprotonation step, whereas the H$_2$O ligand *trans* to the tertiary amino group is of lower acidity.

b. Computational Results. Computational data for the two **1[M(H$_2$O)$_2$]$^{3+}$**complexes agree well with experiments (Table 1), considering the small numerical size of the effects we model. Discussion of these data is provided further below. A qualitative analysis of the interesting stereoelectronic and SO effects, and an evaluation of the periodic trends, is more readily achieved for smaller models. The first set of complexes [M(en)(L)(NH$_3$)$_3$]^q (M = Co, Rh, Ir; en = 1,2-diaminoethane; L = H$_2$O or OH; q = 3+ for L = H$_2$O and q = 2+ for L = OH) (**2[M(H$_2$O)]$^{3+}$/ 2[M(OH)]$^{2+}$**; Figure 2) exhibits one chelate ring and one deprotonable site.[1] Conformational dependencies are furthermore best discussed by opening the chelate ring. In case of M = Co, the conformational dependence of three-bond SO effects has been discussed previously for the simple methyl amine complex **3[M(H$_2$O)]$^{3+}$** (Figure 2). Here we add the ethyl amine complexes **4[M(H$_2$O)]$^{3+}$** (Figure 2) derived from **2[M(H$_2$O)$_2$]$^{3+}$** by opening the 1,2-diaminoethane loop on the other side. This allows the analysis of four-bond pathways for SO-induced shifts.

The Deshielding upon Deprotonation is Caused by SO Shifts. Table 2 lists calculated scalar relativistic and SO ^{1}H shifts for H_A−H_D (see labels in Figure 2) in **2[M(H$_2$O)]$^{3+}$** and **2[M(OH)]$^{2+}$** (M = Co, Rh, Ir). An extended set of results using different ECPs and basis sets can be found in Supporting Information, Table S5. Table 2 shows that at the scalar relativistic level all proton shifts decrease upon deprotonation, usually by ca. 0.4−0.5 ppm, somewhat less for M = Co (cf.

(37) Richens, D. T. *The Chemistry of Aqua Ions*; Wiley: Chichester, UK, 1997.
(38) Düpre, Y.; Bartscherer, E.; Sander, J.; Huch, V.; Hegetschweiler, K. *Z. Kristallogr. New Cryst. Struct.* **1999**, *214*, 407.
(39) A search in the Cambridge Structural Data Base (CSD version 5.28, update Aug. 2007) revealed only a single entry (refcode: DEYHAQ) for a crystal structure containing the [Rh(tren)] fragment. In this structure, the two additional coordination sites are occupied by a chelating Se−CH$_2$−CH$_2$−NH$_2$ ligand. The structural differences to **1[Co(H$_2$O)$_2$]$^{3+}$** are more significant in comparison to **1[Rh(H$_2$O)$_2$]$^{3+}$**. However, the structure still exhibits the same type of conformation of the tren fragment: Nakajima, K.; Kojima, M.; Fujita, J.; Ishii, T.; Ohba, S.; Ito, M.; Saito, Y. *Inorg. Chim. Acta* **1985**, *99*, 143.

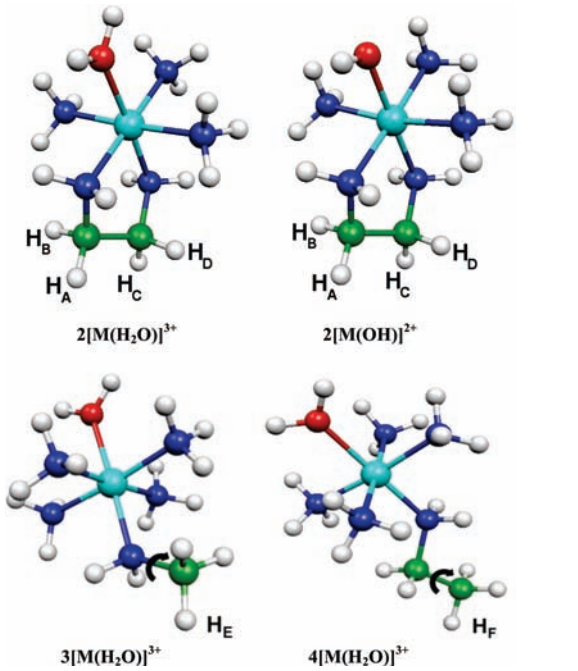

Figure 2. Molecular structures of the aqua complex **2[M(H$_2$O)]$^{3+}$** and its deprotonated counterpart, **2[Co(OH)]$^{2+}$**, as well as open-ring **3[M(H$_2$O)]$^{3+}$** and **4[M(H$_2$O)]$^{3+}$** models.

Figure 3a). This corresponds to a negative slope of the curves in Figure 1 (as observed, e.g., for H_E or H_F). Deshielding upon deprotonation is caused exclusively by differential SO shifts, $\Delta(\delta_{SO})$, which are generally positive, albeit to a widely differing extent (Figure 3b). The most positive differential SO shifts are found for H_C, which belongs to the *trans* CH_2 group and exhibits an antiperiplanar M−N−C−H pathway. Only for this atom the overall differential shifts remain positive after addition of scalar-relativistic (SR) and SO contributions (Figure 3c; this corresponds to a positive slope in Figure 1). In the other cases, overall negative differential shifts at SR level overcompensate the positive differential SO shifts, leading overall to negative "conventional" deprotonation shifts (albeit in some cases with extremely small absolute value; Table 2, Figure 3c).

These observations are consistent with the reported all-electron results[1] for **2[Co(H$_2$O)]$^{3+}$/2[Co(OH)]$^{2+}$**. Obviously, a qualitatively similar behavior holds for the Rh and Ir homologous complexes but with some notable quantitative differences (Table 2, Figure 3): the negative differential shifts before inclusion of SO effects (SR values) increase significantly in absolute value from Co to Rh (less so for H_A) and tend to decrease slightly from Rh to Ir (Figure 3a). The differential SO shifts (Figure 3b) become only slightly more positive from Co to Rh and then increase more noticeably from Rh to Ir (in particular for H_C). Adding the SR shifts and SO contributions together, the nonmonotonous trend in Figure 3c follows (cf. Table 2), which actually exhibits dramatically reduced differential H_C shifts for Rh compared to Co, but larger ones for Ir. Due to the larger SO effects with M = Ir, the absolute values of the overall slightly negative differential shifts of the other hydrogen atoms are very small.

The SO Shifts Do Not Follow a Z^2 Dependence. Table 2 shows clearly that the SO shifts do not follow the conventional Z^2 dependence. Let us concentrate in particular on the absolute SO contributions to the antiperiplanar positions H_C and H_A, where the most notable SO shifts are found. From Co to Rh, only a small increase of maximally 20% (i.e., by a factor of 1.2) is found (both for **2[M(H$_2$O)]$^{3+}$** and **2[M(OH)]$^{2+}$**), while an increase with Z^2 would correspond roughly to a factor of 2.8. Curve fits are provided in Figure S4 in Supporting Information. The relative increase for the SO shifts at H_B and H_D appears larger, but these very small values are in the range of numerical noise of the perturbation procedure and should be viewed with caution. Going from Rh to Ir (again for H_C and H_A) we find generally an increase by a factor of about two (Table 2). This should be compared to factor of roughly three predicted by a Z^2 dependence of SO effects. Overall, we observe a strikingly small increase from Co to Rh and also a too small increase from Rh to Ir. (cf. Figure S4 in the Supporting Information). The similar magnitude of the SO shifts for Co and Rh complexes contradicts all commonly expected trends for spin−orbit effects. Indeed, to our knowledge, this is the first observation of relativistic effects with such an unusual behavior down a group of the Periodic Table for any property studied so far.

The observations may be rationalized by closer inspection of the third-order perturbation expression for σ_{SO}:

$$\sigma_{N,uv}^{SO-I} = \frac{\partial^2}{\partial\mu_{N,u}\partial B_{0,v}} \left[\sum_{m,n\neq 0} \frac{\langle 0|H_{N,u}^{FC} + H_{N,u}^{SD}|m_T\rangle\langle m_T|H^{SO}|n_s\rangle\langle n_s|H_v^{OZ}|0\rangle}{(E_0 - {}^3E_m)(E_0 - {}^1E_n)} + \text{permutations} \right] \quad (1)$$

Here, $\boldsymbol{\mu}$ denotes the nuclear magnetic moment and $\mathbf{B}_0$ the external magnetic field. The total energies E in the denominator pertain to triplet and singlet excited states of the system, and the double sum runs over all excited states. $H_{N,u}^{FC} + H_{N,u}^{SD}$ in the first matrix element denotes hyperfine operators, in the present discussion the Fermi contact operator. The second and third matrix elements account for the SO operator, and for the orbital Zeeman interaction with the external magnetic field, respectively.

We have suggested in ref 1 that the unusually large SO shielding in the cobalt complexes is actually not due to an unusually large SO interaction (i.e., SO matrix elements in the numerator of eq 1) but due to the small denominators in eq 1 corresponding to the small energy gaps between the occupied and virtual molecular orbitals involved in the effect (as compared, e.g., to main-group compounds). Note that the energy differences enter in squared form in this expression. Closer inspection shows that, within this perturbation framework, the electronic excitations with ligand-field character dominate the SO shifts. Thus, one may expect the energy denominators to follow the usual increase of ligand-field splittings from the 3d metal Co to the 4d metal Rh to the 5d metal Ir. Particularly small ligand-field splittings for 3d complexes are caused by the compactness of the 3d shell (due to the lack of a radial node) and by the resulting large Pauli repulsion with semicore shells and stretched-bond situations.[40] These effects are less severe in the less compact 4d shell, resulting in larger ligand-field splittings. Finally, the scalar relativistic expansion of the 5d shell[41] reduces the Pauli repulsion problem further and thus gives even stronger bonds and larger ligand-field splittings.[40] The increase in the SO matrix elements down the group would thus

(40) See, for example: Kaupp, M. *J. Comput. Chem.* **2007**, *28*, 320.
(41) Pyykkö, P. *Chem. Rev.* **1988**, *88*, 563.

Table 2. Computed Absolute and Differential ^{1}H Chemical Shifts (in ppm) of the Methylene Hydrogens (H_A-H_D) in **2[M(H$_2$O)]$^{3+}$** and **2[M(OH)]$^{2+}$** (M = Co, Rh, Ir)[a]

		2[M(H$_2$O)]$^{3+}$				**2[M(OH)]$^{2+}$**				Δ[b]		
M	H	torsion[c]	δ_{SR}	δ_{SO}	$\delta_{SR}+\delta_{SO}$	torsion[c]	δ_{SR}	δ_{SO}	$\delta_{SR}+\delta_{SO}$	$\Delta(\delta_{SR})$	$\Delta(\delta_{SO})$	$\Delta(\delta_{SR}+\delta_{SO})$
Co	H_A	159	4.71	−0.47	4.23	161	4.25	−0.27	3.98	−0.45	+0.20	−0.25
	H_B	−84	3.39	−0.07	3.31	−82	3.11	−0.02	3.09	−0.28	+0.05	−0.23
	H_C	161	4.42	−0.75	3.67	161	4.18	−0.17	4.01	−0.24	+0.58	+0.34
	H_D	−82	3.18	−0.08	3.10	−82	3.07	−0.02	3.05	−0.11	+0.06	0.05
Rh	H_A	160	4.58	−0.57	4.01	163	4.08	−0.32	3.76	−0.50	+0.26	−0.24
	H_B	−83	3.32	−0.17	3.15	−80	2.88	−0.04	2.84	−0.44	+0.12	−0.32
	H_C	162	4.55	−0.80	3.75	162	3.98	−0.20	3.77	−0.57	+0.59	+0.02
	H_D	−81	3.31	−0.17	3.14	−81	2.79	−0.03	2.76	−0.52	+0.14	−0.38
Ir	H_A	160	4.53	−1.15	3.38	162	4.04	−0.75	3.29	−0.49	+0.40	−0.09
	H_B	−83	3.15	−0.43	2.72	−80	2.76	−0.07	2.69	−0.39	+0.36	−0.03
	H_C	162	4.51	−1.57	2.94	162	3.95	−0.40	3.55	−0.57	+1.17	+0.60
	H_D	−82	3.14	−0.41	2.73	−81	2.65	−0.02	2.63	−0.49	+0.40	−0.09

[a] PBE/VTZPP/MDF/HIII results. For hydrogen atom labels, see Figure 2. δ_{SR} indicates shifts at scalar relativistic level, before addition of SO corrections δ_{SO}. [b] Difference between shifts for deprotonated and protonated complexes, δ(**2[M(OH)]$^{2+}$**) - δ(**2[M(H$_2$O)]$^{3+}$**). [c] M−N−C−H torsion angle in degrees (see Figure 2), changed by less than 1 degree upon deprotonation.

be counteracted by trend of increasing energy denominators. The expected trend in the ligand-field splittings is corroborated by computed TDDFT excitation spectra for **2[M(H$_2$O)]$^{3+}$** indicated schematically in Figure 4 (Table S6 in Supporting Information gives numerical data). Indeed, rather small energy denominators occur for Co as compared to the larger excitation energies of the Rh and Ir complexes. The change from Rh to Ir is less dramatic than that from Co to Rh, consistent with experience. These excitations are essentially all of ligand-field character.

Let us now assume that the SO matrix elements grow with Z^2 (i.e., $\langle H_{SO}\rangle \approx Z^2$), and that the Fermi contact matrix elements are roughly constant for the relevant ^{1}H nuclei in the Co, Rh, and Ir complexes. Then one may simplify eq 1 to

$$\sigma_{SO} \approx Z^2/\Delta E^2 \tag{2}$$

where ΔE^2 represents an approximation for the denominators of eq 1. Consequently, we obtain a linear equation

$$(\sigma_{SO}\Delta E^2)^{1/2} \approx Z \tag{3}$$

If the above assumptions are correct, eq 3 should hold for our data. We use an average of the n lowest excitation energies (Table S6) for ΔE^2, that is, $\Delta E^2 = \Sigma_n(\varepsilon_{nT}\ \varepsilon_{nS})/n$, where n = 1, 2,..., 5 and $\varepsilon_{nT} = {}^3E_n - E_0$ and $\varepsilon_{nS} = {}^1E_n - E_0$. Indeed, plotting eq 3 for increasing n, one rapidly converges to a linear dependence, which is shown for n = 5 (ΔE^2 is from now on approximated by the lowest five singlet and triplet excitations) in Figure 5. This is qualitative evidence for a Z^2-dependence of the SO matrix elements "tuned" by the increasing excitation-energy denominators. A rather similar size of δ_{SO} in Co and Rh complexes follows, whereas the smaller growth of the energy denominator from Rh to Ir does not fully compensate the increased SO matrix elements anymore.

Magnitude of ^{1}H SO Shifts Depends on the cis/trans Orientation of the Deprotonation Site as well as on the M−N−C−H Torsion Angle. The trends in δ_{SO} are different in the protonated and deprotonated forms of the complexes. While δ_{SO} for H_C is larger than that for H_A in the aqua complex, the situation is reversed in the deprotonated hydroxy complex (Table 2). This has been traced to the *cis* vs *trans* position of the N−CH$_2$ group in question relative to the deprotonation site.[1] For example, in **2[M(H$_2$O)]$^{3+}$** (Figure 2), H_A and H_B are *cis* and H_C and H_D *trans* relative to the deprotonated aqua ligand. That is, in spite of the antiperiplanar Co−N−C−H conformation of H_A and H_C, the two protons exhibit different behavior for δ_{SO}, due to the *trans* influence of the oxygen donor ligand. Additionally, the M−N−C−H torsion angle α influences δ_{SO} via a Karplus-type relation[1]

$$\sigma_{SO} \approx k_1 \cos 2\alpha + k_2 \cos \alpha + k_3 \tag{4}$$

where the k_n are fitting constants. Figure 6 illustrates both the Karplus relation and the *trans* effect on δ_{SO} for **3[Co(H$_2$O)]$^{3+}$** and **3[Co(OH)]$^{2+}$** (cf. Figure 2) by stepwise rotation of the methyl substituent. It is clear that the absolute SO shifts are largest for the *trans* aqua complex, and the differential SO effect is also largest for the *trans* position.[1] The large reduction of the SO shift in *trans* position for **3[Co(OH)]$^{2+}$** was shown[1] to be due to the weakening and lengthening of the Co−N bond *trans* to the strong hydroxy donor ligand. This diminishes the transfer of the SO-induced spin polarization[2,4,6] to the nucleus in question. Selected bond lengths for the **2[M(H$_2$O)]$^{3+}$** and **2[M(OH)]$^{2+}$** complexes in Table 3 confirm the lengthening of the *trans* M−N bond upon deprotonation. The relatively long *cis* M−N bond actually shortens slightly upon deprotonation. Yet, the corresponding H_A SO shift is not enhanced but even reduced slightly further. This points to additional electronic influences beyond the mere bond-length effect.

Four-Bond Pathway for the Transfer of SO-Induced Spin Polarization. We had previously demonstrated the partial interruption of the three-bond *trans* pathway (see above) upon deprotonation by placing a Fermi-contact finite perturbation at the antiperiplanar methyl proton in **3[Co(H$_2$O)$_2$]$^{3+}$** and **3[Co(OH)$_2$]$^{2+}$**and monitoring the spin density induced by this perturbation.[1] Corresponding plots for H_C in the chelate complexes **2[Co(H$_2$O)]$^{3+}$** and **2[Co(OH)]$^{2+}$** (Figure 7) reveal that, in addition to the three-bond pathway discussed above (right side of the chelate ring in both plots), a four-bond pathway via the *cis* N−CH$_2$ moiety contributes also to the spin-polarization transfer between Co and H_C (left part of the chelate ring). In fact, the spin-density amplitudes suggest that, while the three-bond pathway is diminished upon deprotonation, the four-bond pathway is actually slightly enhanced.

For further analysis, the ethyl amine complexes **4[M(H$_2$O)]$^{3+}$** and **4[M(OH)]$^{4+}$** were considered (cf. Figure 2d). The Co−N−C−C torsion angle in **4[Co(H$_2$O)]$^{3+}$** was kept at 180 degrees for simplicity (the energy minimum is at 178 degrees), and the N−C−C−H torsion angle was changed by rotating the

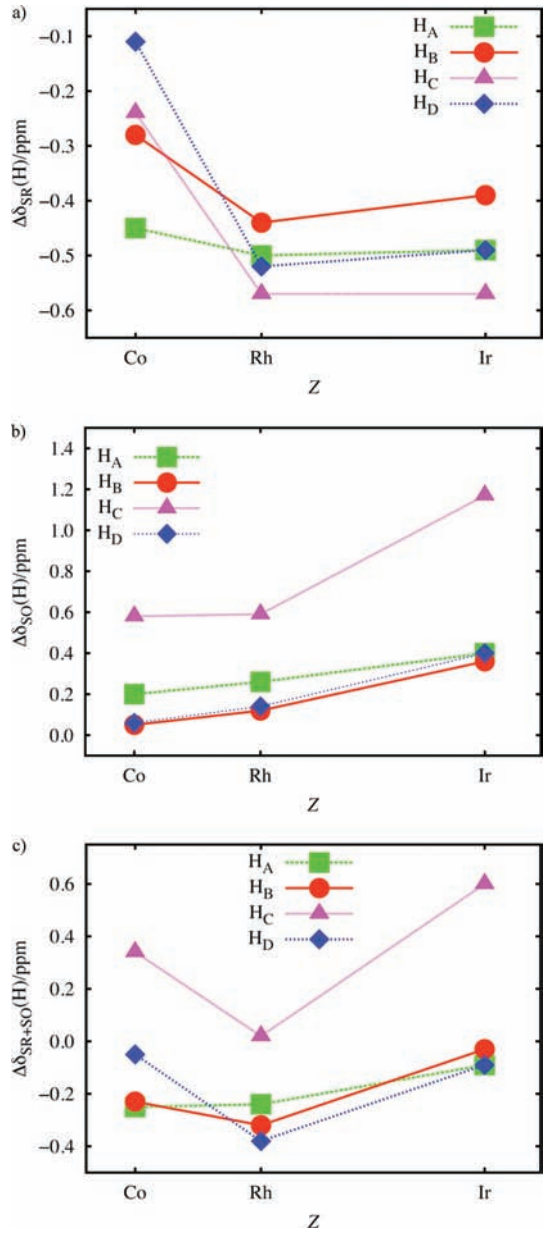

Figure 3. Behavior of the differential ^{1}H chemical shifts ($\mathbf{2[M(OH)]^{2+}} - \mathbf{2[M(H_2O)]^{3+}}$) (M = Co, Rh. Ir) with atomic number *Z*. (a) corresponds to results at scalar-relativistic level (SR), (b) to spin−orbit (SO) contributions, and (c) to the total (SR+SO) differential shift. PBE/MDF/VTZPP/HIII results. See Figure 2 for hydrogen labels.

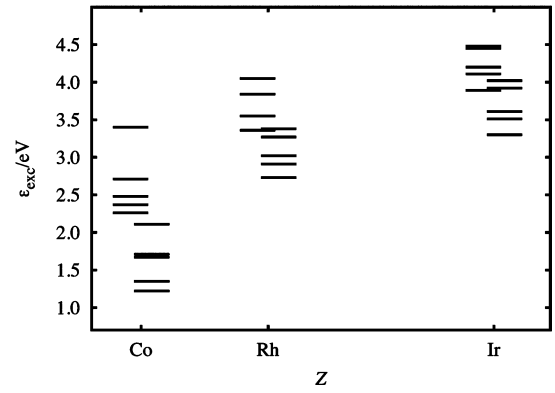

Figure 4. Schematic representation of computed excitation energies of $\mathbf{2[M(H_2O)]^{3+}}$ (M = Co, Rh, Ir) with respect to atomic number *Z*. Stacks of excitation energies shifted to the left/right correspond to singlet/triplet states, respectively. TDDFT-B3LYP/MDF/VTZPP/HIII results (Table S6 in Supporting Information provides the numerical data).

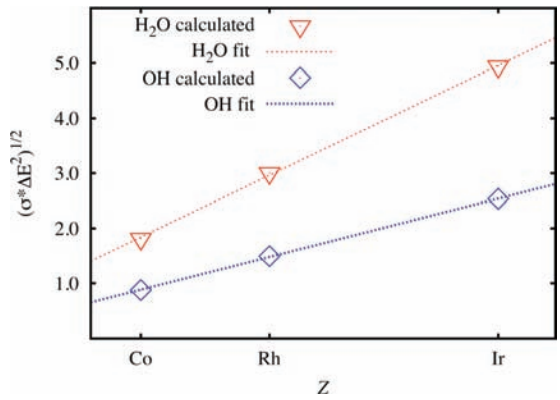

Figure 5. Least-squares fit of eq 3 to calculated (PBE/VTZPP/MDF/HIII) values of σ_{SO} in $\mathbf{2[M(H_2O)]^{3+}}(H_2O)$ and $\mathbf{2[M(OH)]^{2+}}$ (OH^-), M = Co, Rh, Ir, show qualitatively that, while the SO integrals in eq 1 follow the Z^2 dependence on the atomic number, σ_{SO} does not increase due to opposing SO and ligand field splitting effects in eq 1.

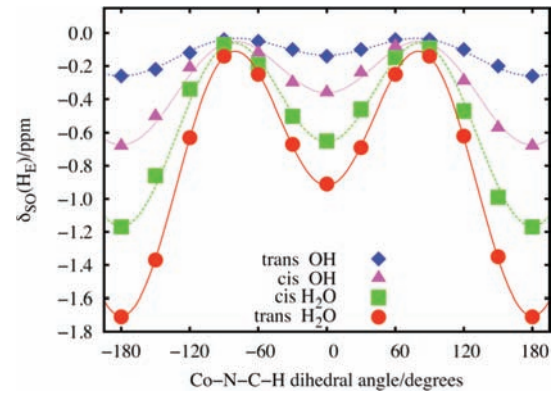

Figure 6. Stereochemical dependencies of ^{1}H SO chemical shifts shown for $\mathbf{3[M(H_2O)]^{3+}}$ and $\mathbf{3[M(OH)]^{2+}}$. The Karplus-type dependence of δ_{SO} on torsion angle, the dependence on *cis* vs *trans* position relative to the deprotonation site, and the effect of deprotonation may be seen. The points are obtained quantum-chemically, the curves are fits of eq 4.

methyl group. Interestingly, the four-bond path makes contributions of similar magnitude to δ_{SO} as the three-bond pathway (Figure 8). However, in contrast to the latter, the former does not follow a simple Karplus relation like eq 4, as observed in Figure 8. The curve is distinctly asymmetrical (with sine character near $\alpha = 0$). The data do not lend themselves to a compact representation. A Fourier series fit of the four-bond data consisting of cosine and sine terms up to the 5α-dependence is provided in Figure 8. With the real chelate ligands the role of the four-bond pathway may be somewhat diminished as compared to the model because the Co−N−C−C torsion angle comes into play. In the chelate complexes of this study, it is usually about 150 degrees, 30 degrees below the value energetically optimal for the $\mathbf{4[M(H_2O)]^{3+}}$ model. There is also a further dependence on the *cis/trans* position of the corresponding four-bond pathway with respect to the deprotonating site, analogous to the three-bond pathway (cf. above).

Understanding the Deprotonation Characteristics of the Experimental $\mathbf{[M(tren)(OH_2)_2]^{3+}}$ Systems. Computed shifts for the experimentally studied tren complexes (Figure 1) are given in Table S7 in Supporting Information (cf. differential shifts in

Table 3. Selected Computed Bond Lengths (in Å) in **2[M(H$_2$O)]$^{3+}$** and **2[M(OH)]$^{2+}$** (M = Co, Rh, Ir) Species[a]

	2[M(H$_2$O)]$^{3+}$			2[M(OH)]$^{2+}$			Δ[b]		
M	M−N$_{trans}$	M−O	M−N$_{cis}$	M−N$_{trans}$	M−O	M−N$_{cis}$	M−N$_{trans}$	M−O	M−N$_{cis}$
Co	1.97	2.05	2.01	2.03	1.88	1.99	+0.07	−0.17	−0.02
Rh	2.06	2.17	2.11	2.16	1.99	2.10	+0.10	−0.18	−0.01
Ir	2.08	2.18	2.13	2.17	2.02	2.12	+0.09	−0.16	−0.01

[a] BP86/def2-TZVPP results. [b] Bond length in **2[M(OH)]$^{2+}$** minus bond length in **[M(H$_2$O)]$^{3+}$**.

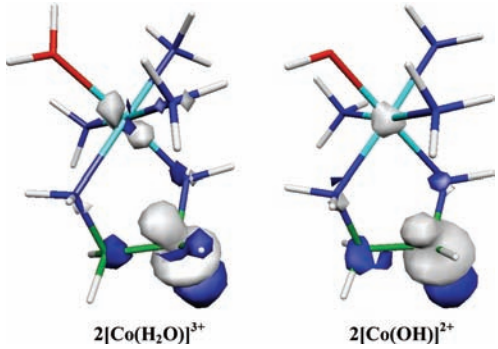

Figure 7. Induced spin densities in **2[Co(H$_2$O)]$^{3+}$** and **2[Co(OH)]$^{2+}$** models using a Fermi-contact perturbation of 0.0005 a.u. at H$_C$ (hidden in the node of the largest spin density) and $\pm 10^{-6}$ a.u. isosurface values. Spin density pathways along H−C−N−Co and H−C−C−N−Co point to transfer of SO-induced spin polarization via both directions.

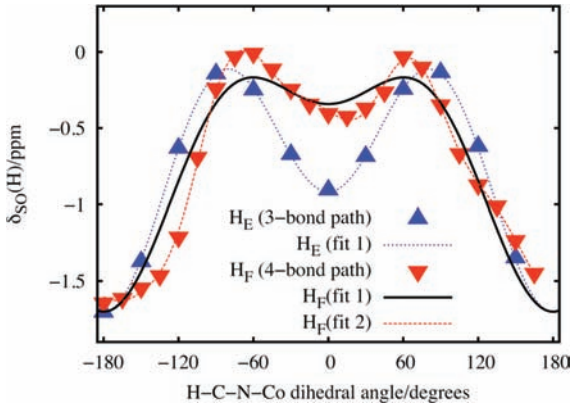

Figure 8. Conformational dependencies of spin−orbit shifts on designated hydrogen atoms in **3[Co(H$_2$O)$_2$]$^{3+}$** and **4[Co(H$_2$O)$_2$]$^{3+}$** (cf. Figure 2), corresponding to three- and four-bond pathways, respectively. Points correspond to the calculated values, curves are fit to eq 4 (fit 1) and to a Fourier series consisting of *cos* and *sin* terms up to the 5α-dependence (fit 2, formula not shown).

Table 1). The calculations tend to overestimate the shifts by about 0.2 to 1 ppm, typically by about half a ppm. The deviations are as expected due to a) the neglect of environmental effects, and b) rovibrational effects, c) the use of a common gauge origin for the SO shifts (the common gauge results are typically ca. 0.2−0.3 ppm higher than the more robust GIAO calculations, see Table S4 in Supporting Information), d) neglect of the spin-dipolar contributions to the SO shifts.[42] However, the errors are expected to cancel out largely for differential shifts and trends, and Table 1 actually shows that the calculations are rather successful for qualitative predictions and for understanding the process of deprotonation. The few notable discrepancies between theory and experiment in Table 1 occur mainly in the cases where the measured differential shifts are very small, and the errors caused by the computational approximations start to play a crucial role.

(42) The concomitant error may reach a few tenths of a ppm for ^{1}H nuclei not directly bonded to heavy atoms (see ref 32a and Straka, M.; Lantto, P.; Räsänen, M.; Vaara, J. *J. Chem. Phys.* **2007**, *127*, 234314).

Table 4. Calculated Differential ^{1}H Chemical Shifts (in ppm) Induced by First (Δ_1) and Second Deprotonation (Δ_2) of the Two Coordinated Water Molecules in **1[M(H$_2$O)$_2$]$^{3+}$** (M=Co, Rh, Ir)

M	H	H−C−N−M[a]	$\Delta_1(\delta_{SR})$	$\Delta_2(\delta_{SR})$	$\Delta_1(\delta_{SO})$	$\Delta_2(\delta_{SO})$	$\Delta_1(\delta_{SR}+\delta_{SO})$	$\Delta_2(\delta_{SR}+\delta_{SO})$
averaged[b]								
Co	H$_A$		−0.79	−0.10	0.51	0.29	−0.28	0.19
	H$_B$		0.05	−0.19	0.29	0.02	0.34	−0.17
	H$_C$		−0.31	0.06	0.12	0.13	−0.19	0.18
	H$_D$		−0.27	−0.06	0.02	0.03	−0.25	−0.03
	H$_E$		−0.73	−0.33	0.12	0.05	−0.61	−0.28
	H$_F$		−0.56	−0.14	0.01	0.02	−0.56	−0.12
Rh	H$_A$		−0.67	−0.34	0.37	0.26	−0.30	−0.08
	H$_B$		−0.40	−0.22	0.24	0.06	−0.16	−0.17
	H$_C$		−0.50	−0.30	0.12	0.16	−0.38	−0.14
	H$_D$		−0.05	−0.43	0.02	0.02	−0.03	−0.42
	H$_E$		−0.57	−0.30	0.21	0.11	−0.36	−0.19
	H$_F$		−0.51	−0.25	0.03	0.05	−0.48	−0.20
Ir	H$_A$		−0.62	−0.31	0.59	0.39	−0.03	0.08
	H$_B$		−0.40	−0.21	0.41	0.16	0.00	−0.05
	H$_C$		−0.47	−0.25	0.22	0.25	−0.25	−0.01
	H$_D$		0.04	−0.41	0.00	0.11	0.04	−0.30
	H$_E$		−0.53	−0.30	0.31	0.26	−0.22	−0.04
	H$_F$		−0.47	−0.23	0.04	0.19	−0.43	−0.03
particular hydrogens[c]								
Co	H$_A$	−168	−0.77	−0.12	0.54	0.24	−0.22	0.13
	H$_A$	168	−0.81	−0.07	0.48	0.33	−0.33	0.26
	H$_B$	−83	0.15	−0.06	0.06	0.01	0.21	−0.05
	H$_B$	161	−0.06	−0.32	0.51	0.03	0.46	−0.29
	H$_C$	146	−0.42	0.00	0.17	0.23	−0.25	0.23
	H$_C$	−99	−0.20	0.11	0.07	0.02	−0.13	0.14

[a] Torsion angle in degrees in the fully protonated form [M(tren)(H$_2$O)$_2$]$^{3+}$. [b] Values correspond to an average of the corresponding hydrogen atoms (Figure 1, Table S9, Supporting Information). [c] Representative data for particular hydrogens before averaging. For complete data set, see Tables S8−S9 in the Supporting Information.

The general principles observed in the calculations on the models in Figure 2 apply to a large extent also for the experimental systems, as seen from the examples in Table 4 (full data are in Tables S7−S9 in Supporting Information). The nonrelativistic or SR shifts decrease typically upon deprotonation, whereas the SO corrections, δ_{SO}, increase (small deshielding already without SO corrections is found for one of the H$_B$ positions in the Co complex, and for H$_D$ in the Rh and Ir complexes). Deshielding upon deprotonation is typically observed when the positive $\Delta\delta_{SO}$ is larger than the negative $\Delta\delta_{SR}$. The SO shifts are large for a three-bond M−N−C−H pathway *trans* to the deprotonation site, particularly when the torsion angle is close to 180 degrees (see selected results in Table 4 or full data in Table S9, Supporting Information).

These insights allow the deduction of the deprotonation sequence from the ^{1}H NMR titration curves (as, e.g., Figure 1). The H$_2$O unit *trans* to the primary amino group is predominantly deprotonated in the first step. This is revealed by the large differential SO shifts for H$_B$ in the first step and for H$_A$ in the second step. Hence, H$_B$ is likely *trans* to the first deprotonation

site and H_A to the second deprotonation site. H_C and H_D in the cobalt complex (Figure 1, bottom) confirm the trend. In general, we may expect that sufficiently large differential SO shifts can provide important information on deprotonation sequences and stereochemistry in more complicated systems.[1] Furthermore, if the approximate structure of a complex is known, the deprotonation shifts can be used in certain cases to distinguish between hydrogen atoms without performing additional 2-D NMR experiments.

The overall situation in the experimentally studied systems is, however, more complex than in the models, as there are two H_2O units to be deprotonated and several three- and four-bond pathways for the transfer of SO induced spin polarization. Also, two different hydrogen atoms with very different torsion angles may contribute to one measured chemical shift (Table 4). The less pronounced deshielding upon deprotonation in the Rh compared to the Co complex (Figure 1) results from relatively similar SO shifts (see above, Table S9, Supporting Information) combined with a more pronounced shielding upon deprotonation at the scalar relativistic level (see also Figure 3 for the results with **2**$[M(H_2O)]^{3+}$). These trends are confirmed by the data for the experimental systems (cf. Table 4 and Table S9, Supporting Information). Table 4 shows finally that, while the SO shifts are clearly predicted to be largest for M = Ir (in particular in the smaller models), the observable differential shifts upon deprotonation may not necessarily be the most positive ones (cf. average value for H_B). This has to do with the above-mentioned averaging and with compensation between the SO contributions and the differential shifts, before adding the SO effects (see also above).

4. Conclusions

We had previously found the partially nonintuitive ^{1}H chemical shift patterns of cobalt polyamine complexes upon deprotonation of aqua or alcohol coligands to be caused by spin−orbit induced spin polarization, transmitted across at least three bonds from the central atom. Here the NMR shifts of these types of complexes have yielded yet another fundamental surprise. While spin−orbit coupling, which is a genuinely relativistic effect, usually increases with the square of the atomic number, the spin−orbit induced ^{1}H shifts of the Co, Rh, and Ir complexes studied here are far from such a behavior. Instead, the spin−orbit shifts stagnate from Co to Rh and also increase less than expected from a Z^2 behavior from Rh to Ir. To our knowledge, these are the first results of spin−orbit effects on any molecular property with such an unusual dependence on nuclear charge. The slow growth down the group may be rationalized by the counteracting trend in the ligand-field splittings, which enters the perturbation expression for the spin−orbit shifts. Small energy denominators explain also why ^{1}H spin−orbit shifts of about 1 ppm may be caused via three or more bonds by a comparably light atom like cobalt.

The computational studies have been confirmed clearly by comparative ^{1}H NMR titrations of the homologous complexes $[M(tren)(OH_2)_2]^{3+}$ (M = Co, Rh). The overall deprotonation shifts measured and computed for the Rh complex are actually less "nonclassical" than for its homologous Co complex. This has been traced back to a more pronounced partial cancellation of the (similarly large) spin−orbit induced differential shifts by other differential shift contributions upon deprotonation. The computations predict furthermore larger spin−orbit effects for the Ir complexes, but the overall differential shift patterns may actually be most characteristic for the lightest member of the series, Co.

The previous analyses of the deprotonation-shift patterns had revealed a pronounced conformational dependence of the spin−orbit shifts via a Karplus-like behavior of a three-bond pathway for the transfer of spin−orbit-induced spin polarization. Closer analysis has now revealed a pronounced four-bond pathway along the other side of a given chelate ring, which contributes also significantly to the spin−orbit shifts. Together with a strong *cis* - *trans* dependence, these spin−orbit induced shift contributions allow substantial insight into the stereochemistry of the complexes and the coordinated ligands and may even be used for spectra assignment.

Acknowledgment. Dedicated to Professor Pekka Pyykkö for his seminal achievements in the theory of NMR parameters. The X-ray data have been collected by Dr. V. Huch, and the crystal structure has been solved and refined by Dr. S. Stucky (both at Saarland University). We thank Ms. Anne Jung (Saarland University) for a valuable contribution to the synthesis of $[Rh(tren)(OH_2)_2](CF_3SO_3)_3$. We thank Profs. M. Dolg (Cologne) and H. Stoll (Stuttgart) for providing us with the multiconfiguration Dirac−Fock ECPs. Dr. D. Figgen (Massey University, Auckland) and Prof. K. Peterson (Washington State University, Pullman) are acknowledged for providing their basis sets prior to publication. The project was supported by a Marie Curie Intra-European Fellowship (M.S.) within the sixth European Community Framework Program and by the European Reintegration Grant (M.S) within the seventh European Community Framework Program. M.S. was further supported by the Czech Science Foundation (grants no. 203/09/2037 and 202/07/0732) and by the Academy of Sciences of the Czech Republic (grant no. IAA400550701 and IAA40550705). M.H. and J.V. are with the Finnish Center of Excellence in Computational Molecular Science. The Emil Aaltonen Foundation and Magnus Ehrnrooth foundations are gratefully acknowledged for further financial support. Work in Würzburg was supported by Deutsche Forschungsgemeinschaft (KA 1187/5-2). Computational resources were in part supplied by CSC Scientific Computing, Ltd, Espoo, Finland.

Supporting Information Available: Tables S1 and S2 list NMR titration results for **1**$[Rh(H_2O)_2]^{3+}$ and crystal data for $[Rh(tren)Cl_2]_2[ZnCl_4]\cdot 2H_2O$, respectively. Table S3 gives details on the basis sets used. Table S4 details the dependence of the computational results for **2**$[M(H_2O)]^{3+}$ on the exchange-correlation functional and basis set. Table S5 lists the dependence of the results for **2**$[M(H_2O)]^{3+}$ and **2**$[M(OH)]^{2+}$ at the PBE level, with different metal basis sets and ECPs. Table S6 lists the TDDFT excitation energies of **2**$[M(H_2O)]^{3+}$ and **2**$[M(OH)]^{2+}$. Tables S7−S9 give the computed chemical shifts and differential shifts for the full tren complexes. Figures S1−S2 show measured and calculated ^{1}H NMR spectra for **1**$[M(H_2O)_2]^{3+}$ and **1**$[M(OH)_2]^{+}$, as well as the crystallographically determined structure of *cis*-$[Rh(tren)Cl_2]^{+}$. Figure S3 compares molecular structures of *cis*-$[Rh(tren)Cl_2]^{+}$ and *cis*-$[Co(tren)(OH_2)_2]^{3+}$. Figure S4 shows fits of spin−orbit chemical shifts against Z^2. Complete refs 22 and 31. This material is available free of charge via the Internet at http://pubs.acs.org.

JA903637M